Band-gap measurements of bulk and nanoscale hematite by soft x-ray spectroscopy

B. Gilbert,[1] C. Frandsen,[2] E. R. Maxey,[3] and D. M. Sherman[4]
[1]*Earth Sciences Division, Lawrence Berkeley National Laboratory, MS 90R1116, 1 Cyclotron Road, Berkeley, California 94720, USA*
[2]*Department of Physics, Technical University of Denmark, DK-2800 Kongens Lyngby, Denmark*
[3]*Argonne National Laboratory, APS-XSD-XOR-CEP-11ID B, Building 433, Room D-009, 9700 South Cass Avenue, Argonne, Illinois 60439-4814, USA*
[4]*Department of Earth Sciences, University of Bristol, Bristol BS8 1RJ, United Kingdom*
(Received 16 June 2008; revised manuscript received 28 September 2008; published 12 January 2009)

Chemical and photochemical processes at semiconductor surfaces are highly influenced by the size of the band gap, and ability to control the band gap by particle size in nanomaterials is part of their promise. The combination of soft x-ray absorption and emission spectroscopies provides band-gap determination in bulk and nanoscale itinerant electron semiconductors such as CdS and ZnO, but this approach has not been established for materials such as iron oxides that possess band-edge electronic structure dominated by electron correlations. We performed soft x-ray spectroscopy at the oxygen *K*-edge to reveal band-edge electronic structure of bulk and nanoscale hematite. Good agreement is found between the hematite band gap derived from optical spectroscopy and the energy separation of the first inflection points in the x-ray absorption and emission onset regions. By applying this method to two sizes of phase-pure hematite nanoparticles, we find that there is no evidence for size-driven change in the band gap of hematite nanoparticles down to around 8 nm.

DOI: 10.1103/PhysRevB.79.035108 PACS number(s): 73.22.−f

I. INTRODUCTION

Hematite, α-Fe_2O_3, is the most common iron oxide in nature, and detailed understanding of electronic and magnetic properties of this material remains of considerable interest. Hematite nanoparticles have potential technological applications[1] and are found in certain terrestrial[1,2] and possibly Martian[3] environments. Numerous investigators have studied the chemical and physical properties of iron oxide particles as a function of particle size with complementary methods such as static[4,5] or ultrafast[6–8] optical spectroscopies, x-ray[9] and Mössbauer[10] spectroscopies, neutron scattering,[11] and tests of (photo)chemical[12,13] or catalytic[14] reactivity. Some of these studies have concluded that small particle size may alter the energy positions of the electronic states that define the semiconductor band gap.[5,9,12,13] Band-gap widening is a striking signature of quantum confinement that has been observed in numerous semiconductor materials possessing delocalized electronic states close to the Fermi level.[15] Enlarging the semiconductor band gap in nanoscale iron oxides would be of considerable importance for the use of this material in solar cells.[16] However, the band-edge electronic structure of iron oxides is dominated by strongly localized Fe 3*d* states unlikely to experience spatial confinement even in nanoscale particles.[17,18] Nevertheless, size, structure, and electronic properties are interrelated in nanoparticles, and the motivation of this study is to establish whether there are any size-dependent trends in the electronic structure of hematite that may explain the published results. We used synchrotron high-energy x-ray scattering and soft x-ray spectroscopy to study the structure and electronic properties of hematite samples of three particle sizes. Soft x-ray spectroscopy is well suited to investigate the electronic structure of bulk and nanoscale materials,[19–21] and we employed oxygen *K*-edge absorption and emission spectroscopies to study valence-band and conduction-band electronic structures. While bulk hematite has been previously studied by O *K*-edge absorption and emission spectroscopies,[22–25] we are not aware of similar studies of hematite nanoparticles.

II. MATERIALS AND METHODS

A. Hematite nanoparticle synthesis

There are few methods for synthesizing hematite nanoparticles with chemical control of particle size. Nanoscale Fe_2O_3 is usually synthesized by an aqueous hydrolysis procedure in which a ferric iron oxyhydroxide precursor phase is dehydrated hydrothermally.[26,27] As a consequence, as observed by us and by Hansen *et al.*,[10] low-temperature processing can lead to material that is not phase pure. We used a multistage wet-chemistry synthesis procedure adopted from Sugimoto *et al.*[28] which produces approximately pure hematite particles with diameters between 5–10 nm. The particles were confirmed to be single phase by the Mössbauer spectroscopy. The particles were washed and freeze dried before subsequent analyses. The characterization of a similar "as-prepared" sample by the Mössbauer spectroscopy, transmission electron microscopy, x-ray, and neutron diffraction is described in Ref. 29 and discussed below. Samples of ~30 nm diameter hematite nanoparticles were produced by annealing commercial NANOCAT ultrafine Fe_2O_3 (MACH I, Inc., King of Prussia, PA) in air at 220 °C. A sample of natural bulk hematite was purchased from Rocko Minerals (Margaretville, NY).

B. Optical spectroscopy

A Cary 5G UV-vis-NIR spectrometer was used to acquire diffuse reflectance spectra from dried powders mounted on Teflon tape. The reflectivity data was converted to the Kebulk-Munk remission function, $F(R)$, defined by $F(R)=(1-R)^2/2R$, where R is the reflectance.

TABLE I. Hematite unit-cell parameters and particle size obtained from x-ray diffraction data.

	Bulk hematite	30 nm Fe_2O_3	8 nm Fe_2O_3	Error
a(Å)	5.027	5.028	5.028	0.003
c(Å)	13.732	13.737	13.769	0.004
Particle diameter (nm)	>100	29	7.8	
Morphology	Sphere	Sphere	Prolate spheroid	

C. X-ray diffraction analysis

We performed powder x-ray diffraction (XRD) at the Advanced Light Source (ALS), Lawrence Berkeley National Laboratory, beamline 11.3.1, to determine the unit-cell parameters in bulk and nanoscale hematite. Dried powders were mounted on Kapton, and XRD was performed in transmission using a two-dimensional (2D) detector. The scattering geometry was calibrated using a LaB_6 standard, and the 2D data were integrated to one-dimensional (1D) data using FIT2D.[30] Instrument resolution was estimated using a National Institutes of Standards and Technology silicon standard. XRD data were analyzed using the MAUD code to refine hematite unit-cell parameters as well as particle size and shape parameters.[31]

D. Pair distribution function analysis

We acquired wide-angle x-ray scattering data at 90 keV from powdered samples placed inside a hollow Kapton tube at beamline 11-ID-B of the Advanced Photon Source (APS) at Argonne National Laboratory using a Mar 2D image plate detector. We acquired between 40 and 100 2 or 5 min exposure from an empty tube and each sample, using FIT2D, to calibrate the detector geometry using data acquired from a CeO_2 reference and to bin each 2D pattern onto a 1D q axis. The structure factor for each iron oxide was obtained using procedures written in the IGORPRO package that subtract the Kapton data and the coherent and Compton atomic scattering contributions. The pair distribution function (PDF) was generated by applying a sine transformation to the q-weighted data up to $q_{max}=25$ Å^{-1} and was analyzed using the PDFGUI code[32] to fit the structural and disorder parameters of bulk hematite to the real-space data between 1–32 Å. The finite data resolution parameter and quadratic correlated atomic motion term were obtained from the fit to the bulk hematite data and kept fixed during analysis of the nanoparticle samples.

E. Soft x-ray absorption and emission spectroscopies

Portions of finely ground bulk hematite and hematite nanoparticles were pressed into indium for soft x-ray spectroscopy analysis under vacuum. Oxygen K-edge x-ray absorption and resonant x-ray emission studies with threshold excitation were performed at beamline 7.0 at the ALS. The incident x-ray energy resolution was set to approximately 0.2 and 0.35 eV for absorption and emission spectroscopies, respectively. The x-ray emission spectrometer has a resolution of about 0.5 eV.[33] In addition, O K-edge emission spectroscopy of bulk hematite was performed at ALS beamline 8.0 as a function of photon energy with similar energy resolution.

The absorption spectra were acquired in fluorescence yield and were calibrated by applying a linear transformation to the energy axis to align the spectrum obtained from a TiO_2 (anatase) standard to a published reference.[34] Following this correction, the inflection point of the onset of the bulk hematite absorption spectrum was measured to be 529.7 eV, in good agreement with a recent study.[21] The absolute energy calibration of the emission x-ray spectrometer was determined with reference to the Zn $L_{2,3}$ emission lines from a zinc metal standard. The absorption spectra were normalized for the energy dependence of incident-beam intensity by the division of a gold grid electron yield signal acquired simultaneously with the sample and then scaled to unity step jump at 552.5 eV. The x-ray emission spectroscopy (XES) spectra were normalized to a constant maximum intensity.

III. RESULTS AND DISCUSSION

A. Nanoparticle size and morphology

Table I shows the results of particle size analysis derived from peak width broadening in the XRD data (Fig. 1). The air-annealed iron oxide powder consisted of spherical particles of mean diameter 30 nm. No information was obtained as to the size distribution, which is expected to be broad. The best-fit particle morphology for the smallest nanoparticles was a spheroid elongated along the c axis with a minor axis diameter of about 8 nm. This finding is consistent with prior studies of hematite nanoparticles prepared using the same synthesis method, as described in Ref. 29. Transmission electron microscopy (TEM) imaging showed individual particles to be spherical with a diameter in the range of 5–10 nm. However, hematite nanoparticles can grow by oriented aggregation to form single crystals that are elongated in the c-axis direction. Neutron-scattering studies showed that approximately one-third of the crystallites are joined in this manner, forming grains possessing an antiferromagnetic domain size of about three particle diameters along the c axis.

B. Structural analyses

Analysis of the XRD data (Fig. 1 and Table I) revealed that relative to bulk hematite and 30 nm hematite particles the dominant structure modification in particles less than 10 nm in diameter is a small (0.2%) enlargement of the unit-cell c parameter, causing a detectable shift in diffraction peak position [inset in Fig. 1(a)]. Figure 2 presents the PDF data obtained from high-energy x-ray scattering data from all

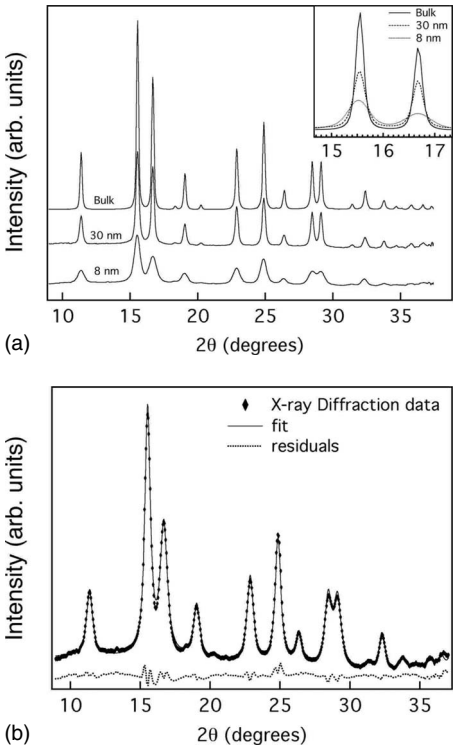

FIG. 1. Synchrotron powder XRD. (a) Comparison of all XRD data. The inset shows a detectable lattice expansion in the smallest particles that is quantified by unit-cell refinement. (b) Experimental and simulated XRD patterns for the best-fit results of unit-cell refinement to the 8 nm nanoparticle data.

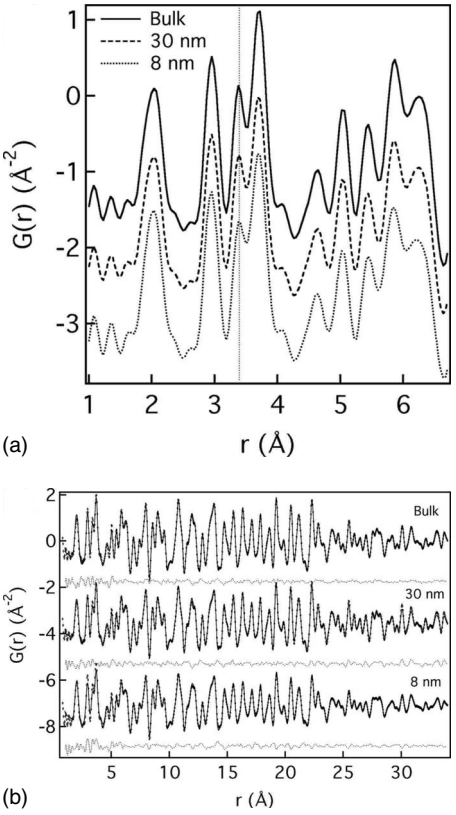

FIG. 2. PDF analysis of the real-space structures of bulk and nanoscale hematite. (a) Stacked plot of the short-range region of the PDF curves. The vertical bar at approximately 3.4 Å highlights the third shell (Fe-O) correlations that are slightly broadened in the 8 nm nanoparticles. (b) Experimental (markers) and best-fit (dark line) PDF for all samples. Residuals (dashed line) are given below each pattern.

samples. Iron oxide synthesis in aqueous media can additionally form a fraction of a disordered nanoscale phase that is difficult to identify in XRD data but which leads to the appearance of peaks in the PDF pattern at short range that are not consistent with the hematite structure. This is not observed in any of the nanoparticle data, indicating that the samples are pure hematite. There are few signs of structural modifications in the hematite nanoparticles relative to the bulk material. PDF peak broadening in the short-range structure is perceptible at the second Fe-O shell as indicated in Fig. 2(a); an effect that is also associated with the larger values of the fit residuals for interatomic distances below 5 Å given in Fig. 2(b). This figure also shows that the attenuation of PDF peak intensity with increasing interatomic distance is slightly greater for the 8 nm sample, consistent with the smaller particle size.[35]

Table II reports the results of fitting a structural model based on the hematite unit cell to the PDF data. While the fitted cell parameters are systematically larger than those obtained from analysis of the diffraction data, the trend with size is identical. Because experimental structure factors can be affected by asymmetric instrumental broadening effects that are not removed before PDF generation, the lattice parameters obtained by the PDF analysis are usually not identical to those obtained by the Rietveld refinement of the diffraction data, which more accurately incorporates instrumental contributions to diffraction peak profiles.[36] The trends in the fitted isotropic disorder factors for the oxygen and iron sites are difficult to interpret. The 30 nm particles have the lowest disorder, likely resulting from the annealing step, while the metal site disorder is greatest in the 8 nm particles. The unexpected drop in oxygen site disorder in these samples likely indicates the presence of short-range strain not accounted for in the single unit-cell fitting approach.

TABLE II. Structural parameters for bulk and nanoscale hematite obtained by analysis of the PDF data. We fitted the hematite unit-cell a and c parameters, the isotropic thermal factors, σ, for iron and oxygen atoms, and the mean iron-oxygen bond lengths, $\langle r_{\text{Fe-O}} \rangle$, calculated from the best-fit unit cell.

	Bulk hematite	30 nm Fe_2O_3	8 nm Fe_2O_3	Error[a]
a (Å)	5.045	5.041	5.041	0.004
c (Å)	13.781	13.775	13.810	0.016
σ_{Fe} (10^{-3} Å^2)	5.7	5.3	6.5	0.6
σ_{O} (10^{-3} Å^2)	15.3	14.4	12.0	4.9
$\langle r_{\text{Fe-O}} \rangle$	1.948	1.947	1.947	0.002

[a]The reported errors (standard deviations) were approximately the same for each of the samples.

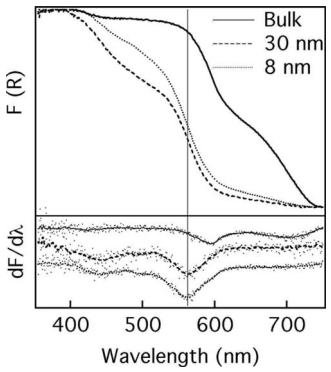

FIG. 3. The Kebulka-Munk function, $F(r)$, obtained from UV-visible diffuse reflectance spectra of powders of bulk and nanoparticulate hematite. The vertical line indicates the inflection point in the nanoparticle absorption spectra determined from the first derivative plotted below, which lies at 562 nm (2.2 eV).

C. Optical spectroscopy

Iron *dd* excitations and Fe-Fe pair excitations that occur throughout the visible photon energy range typically obscure the band-gap transition in optical-absorption spectra of hematite.[37] The hematite band gap is more clearly discernable from measurements of photocurrent vs wavelength, and values of 2.14–2.2 eV for bulk samples are typical.[38,39] As shown in Fig. 3, diffuse reflectance spectra of both 30 and 8 nm hematite exhibit an absorption threshold with an inflection point at 2.2 eV that we attribute to band-gap excitation. The equivalent spectrum from a sample of natural hematite does not exhibit an absorption threshold at this wavelength. However, the observed absorption onset of ~1.8 eV is attributed to charge-transfer excitations at coupled Fe^{2+}-Ti^{4+} impurities that are commonly found in natural hematite and which mask the intrinsic band gap.[40] Thus, the data of Fig. 3 indicate that the optical band gaps of samples that are around 30 or 8 nm in diameter are identical, and we tested this conclusion with x-ray spectroscopy.

D. X-ray absorption and nonresonant emission spectroscopy of bulk hematite

Soft x-ray spectroscopy at the O K-edge ($1s \rightarrow 2p$ excitations) can be an accurate approach for revealing density of states in transition-metal (TM) oxides because the ligand core hole created by photoexcitation is highly screened from the band-edge electronic states localized on the metal sites.[22,24] Such screening lowers the complexity of the absorption spectra relative to TM L-edge ($2p \rightarrow 3d$) spectroscopy and reduces core hole effects on the energy positions of the excited states. Figure 4 shows O K-edge x-ray absorption spectroscopy (XAS) and nonresonant XES data for bulk hematite that may be interpreted using prior theoretical studies.[17,18] The characteristic pre-edge doublet in the absorption spectrum represents transitions to the unoccupied e_g and t_{2g} states. The nonresonant emission spectrum is derived from valence-band (VB) states possessing O $2p$ character. Occupied antibonding Fe $3d$-O $2p$ states lie at the top of the VB, which additionally contains nonbonding O $2p$ states,

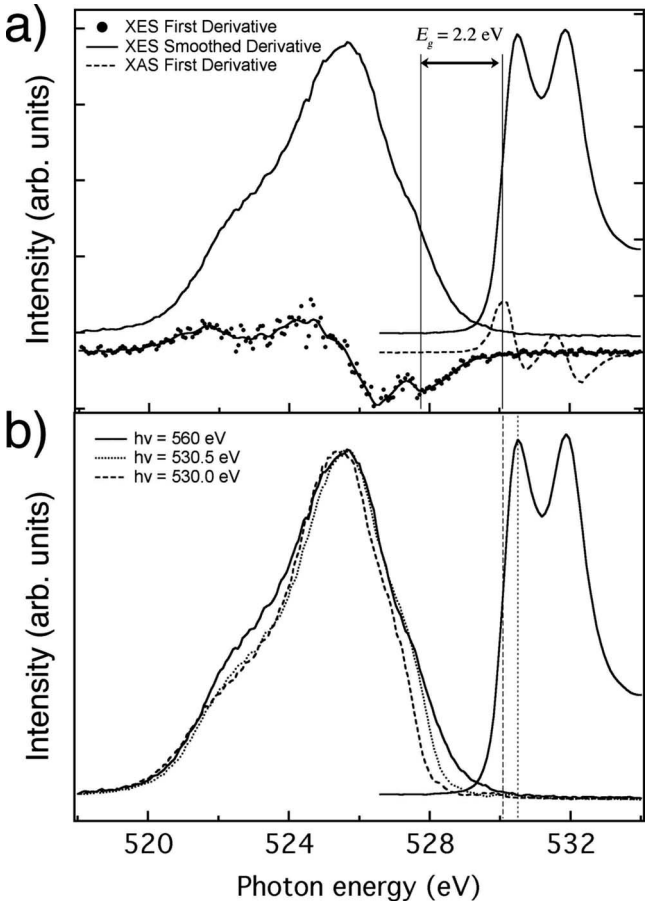

FIG. 4. Soft XAS and XES of bulk hematite at the oxygen K edge. (a) The bulk hematite band gap, E_g, is determined from the XAS and nonresonant XES spectra by taking the derivative to locate the inflection points in the valence-band and conduction-band onsets. Using this approach, E_g=2.2 eV. (b) O K-edge XAS and resonant and nonresonant XES.

and Fe-O bonds formed from O $2p$ and Fe $3d$, $4s$, and $4p$ orbitals.

We tested several strategies for estimating the bulk hematite band gap using the data of Fig. 4. In previous studies of semiconductors such as CdS and ZnO, the VB maximum (VBM) and conduction-band (CB) minimum were identified as the band onset energy in, respectively, the emission and absorption data[41,42] or were found by projecting to the abscissa a linear fit to the threshold regions.[19,20] We find neither approach to be appropriate for iron oxide because both indicate the band gap to be less than 1 eV, significantly less than the commonly accepted value (approximately 2.2 eV). Taking an alternative approach, the energy gap between the first inflection points of the XES and XAS spectra is measured to be 2.2 eV, in agreement with the inflection point of the optical-absorption spectrum (Fig. 3). Thus, we propose this method as an internally consistent approach for determining the band gap from optical or x-ray spectroscopy of iron oxide and possibly for other semiconductors for which the band gap is defined by partially occupied d states. It is clear that VB states appear within the 2.2 eV gap, and lower-energy excitations are also evident in the optical spectra. However,

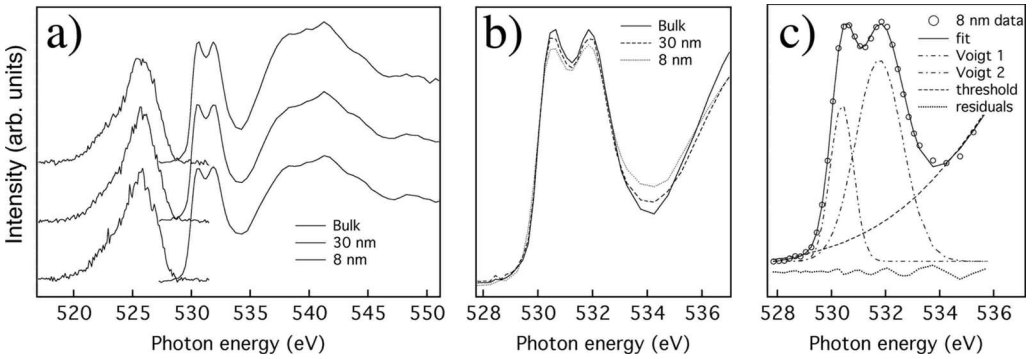

FIG. 5. Oxygen *K*-edge XES and XAS of bulk hematite and Fe_2O_3 nanoparticles. (a) Comparison of XAS and XES data stacked vertically for clarity. (b) Comparison of the XAS pre-edge region. (c) Example peak fit to the pre-edge for the 8 nm nanoparticle sample.

photoexcitation of hematite below 2.2 eV is not reported to cause detectable photoconductivity, and hence we conclude that excitations involving these VB states do not lead to efficient charge separation possibly due to extremely rapid recombination rates.[6]

E. Resonant x-ray emission spectroscopy of bulk hematite

X-ray emission spectra acquired on an absorption resonance can contain energy-loss features due to coherent two-photon resonant Raman processes frequently called resonant inelastic x-ray scattering (RIXS).[43] RIXS processes are not subject to single-photon dipole selection rules and thus can excite electronic transitions that are forbidden in optical-absorption spectroscopy. Hematite and manganosite (MnO) are both $3d^5$ TM oxides, and metal *L*-edge RIXS measurements of these materials observe strong *dd* excitations.[44,45] However, neither the validity nor accuracy of metal atom RIXS for band-gap determination in TM oxides have been fully established. A Fe *L*-edge RIXS study of single-crystal hematite attributed a weak RIXS peak at ~2 eV to be the bulk band gap.[44] However, in a study of hematite nanorods, the same feature was weak or absent and a higher-energy peak was attributed to band-gap excitations.[9] Moreover, the published RIXS spectra exhibit discrepancies in emission energy calibration.

Oxygen *K*-edge emission spectra can also be acquired in a resonant mode although oxygen RIXS of hematite do not excite Fe *dd* transitions.[46,47] Figure 4(b) shows bulk hematite valence-band XES data acquired with nonresonant excitation (560 eV) and acquired resonantly at the XAS onset (530 eV) and on the e_g peak (530.6 eV). The dominant trend is a loss of intensity at the VBM as the excitation energy is decreased. This trend strongly implies that hematite is an indirect gap semiconductor, as previously concluded by Dare-Edwards *et al.*[39] and as found in the isostructural d^0 oxide corundum (α-Al_2O_3).[48] As a coherent two-photon process, a RIXS excitation must satisfy momentum conservation. Since the photon momentum is negligible, the band-gap excitations probed by RIXS are constrained to vertical transitions between bands in energy-momentum plots.[49] Loss of intensity at the VB maximum is observed when the excitation is tuned to the lowest point of the CB because indirect band-gap excitations are forbidden.[50] For direct-gap semiconductors, an opposite trend is found.[51]

F. Band-edge electronic structure in bulk and nanoscale hematite

Figure 5 reports the XAS and on-threshold resonant XES data for bulk hematite and hematite nanoparticles. Very small changes in the threshold region are visible in the low-noise XAS data in Fig. 5(b), and the half-intensity values were obtained from the bulk and nanoparticle data (Table III) by peak fitting to the pre-edge region as shown in Fig. 5(c). The noise on the XES data limits the accuracy with which the energy positions of the VB maxima may be determined to approximately 0.1 eV, and there are no detectable shifts greater than this. Table II summarizes quantitative measures of VB and CB positions. From this, we find that there is no change in band gap in either of the nanoparticulate samples.

G. Metal-ligand hybridization in bulk and nanoscale hematite

As shown in Fig. 5(b), when the XAS spectra are scaled to unity edge jump there is a slight decrease in pre-edge peak heights with decreasing particle size. The fitting results sum-

TABLE III. Results of peak fitting to the pre-edge region of the oxygen *K*-edge absorption spectra.

	Bulk hematite	30 nm Fe_2O_3	8 nm Fe_2O_3
Peak 1 position (eV)	530.43	530.42	530.38
Peak 2 position (eV)	531.82	531.79	531.76
Splitting (eV)	1.39	1.37	1.38
Peak 1 FWHM (eV)	0.96	0.96	1.00
Peak 2 FWHM (eV)	1.96	1.88	2.04
Peak 1 area	0.36	0.35	0.32
Peak 2 area	0.90	0.81	0.83
CBM[a] (eV, ±0.01)	529.95	529.94	529.88
VBM (eV, ±0.1)	527.7	527.7	527.7
Band gap (eV, ±0.1)	2.2	2.2	2.2

[a]The low-energy onset is defined as the position of the first peak minus one half of the full width at half maximum (FWHM).

marized in Table II show that this caused both by an increase in peak width as well as the loss of integrated intensity. Across the series of TM oxides, the O *K*-edge prepeak intensities are inversely related to Fe $3d$ occupation,[22] but all hematite samples studied here are $3d^5$. However, the extent of metal-oxygen hybridization can also affect the strength of charge-transfer-type electronic transitions. It was recently shown that laser excitation of coherent phonon modes in maghemite (γFe_2O_3) leads to oscillations in transient absorption strength,[52] an effect attributed to oscillations in Fe *d*-O *sp* orbital overlap. Moreover, Zou and Volkov[7] identified changes in metal-ligand hybridization in maghemite nanoparticles. Thus, the XAS data provide additional evidence for a slight reduction in the extent of metal-oxygen hybridization in hematite nanoparticles, possibly associated with the small lattice expansion observed in this study.

IV. CONCLUSIONS

The combination of x-ray absorption and emission spectroscopies at the oxygen *K* edge can be used for band-gap determination in iron oxides. Good agreement is found between the hematite band gap derived from optical spectroscopy and the energy separation of the first inflection points in the x-ray absorption and emission onset regions. However, further theoretical and experimental works are required to fully understand the nature of the band gap in *d*-electron semiconductors and the band-gap excitations probed by soft x-ray spectroscopy. We find that there is no evidence for size-driven change in the band gap of hematite nanoparticles down to around 8 nm.

ACKNOWLEDGMENTS

We thank Wayne Lukens for assistance with the UV-vis diffuse reflectance measurements and Glenn Waychunas for the sample of natural hematite. Soft x-ray absorption and emission studies were performed at beamlines 7.0.1 and 8.0.1 of the ALS, and we thank Jinghua Guo and Jonathan Denlinger. Synchrotron powder-diffraction data were acquired at ALS beamline 11.3.1, and we thank Simon Teat. The high-energy x-ray scattering data were acquired at beamline 11-ID-C at the APS, and we thank Peter Chupas. B.G. was supported by the Director, Office of Science, Office of Basic Energy Sciences, of the U.S. Department of Energy, hereby abbreviated to DOE-BES, under Contract No. DE-AC02-05CH11231. Use of the ALS and the APS is supported by DOE-BES under Contracts No. DE-AC02-05CH11231 and No. W-31-109-ENG-38, respectively.

[1] V. A. Drits, B. A. Sakharov, A. L. Salyn, and A. Manceau, Clay Miner. **28**, 185 (1993).
[2] K. Dideriksen, B. C. Christiansen, J. A. Baker, C. Frandsen, T. Balic-Zunic, E. Tullborg, S. Morup, and S. L. S. Stipp, Chem. Geol. **244**, 330 (2007).
[3] R. V. Morris, D. C. Golden, J. F. Bell III, H. V. Lauer, Jr., and J. B. Adams, Geochim. Cosmochim. Acta **57**, 4597 (1993).
[4] M. Iwamoto, Y. Tachibana, and T. Abe, J. Mol. Catal. A: Chem. **155**, 143 (2000).
[5] Y. P. He, Y. M. Miao, C. R. Li, S. Q. Wang, L. Cao, S. S. Xie, G. Z. Yang, B. S. Zou, and C. Burda, Phys. Rev. B **71**, 125411 (2005).
[6] N. J. Cherepy, D. B. Liston, J. A. Lovejoy, H. Deng, and J. Z. Zhang, J. Phys. Chem. B **102**, 770 (1998).
[7] B. S. Zou and V. Volkov, J. Phys. Chem. Solids **61**, 757 (2000).
[8] L. Fu, Z. Wu, X. Ai, J. Zhang, Y. Nie, S. Xie, G. Yang, and B. Zou, J. Chem. Phys. **120**, 3406 (2004).
[9] L. Vayssieres, C. Sathe, S. Butorin, D. K. Shuh, J. Nordgren, and J. Guo, Adv. Mater. (Weinheim, Ger.) **17**, 2320 (2005).
[10] M. F. Hansen, C. B. Koch, and S. Mørup, Phys. Rev. B **62**, 1124 (2000).
[11] S. Mørup, D. E. Madsen, C. Frandsen, C. R. H. Bahl, and M. F. Hansen, J. Phys.: Condens. Matter **19**, 213202 (2007).
[12] S. Chatterjee, S. Sarkar, and S. N. Bhattacharyya, J. Photochem. Photobiol., A **72**, 183 (1993).
[13] K. Cheng, Y. P. He, Y. M. Miao, B. S. Zou, Y. G. Wang, T. H. Wang, X. T. Zhang, and Z. L. Du, J. Phys. Chem. B **110**, 7259 (2006).
[14] A. S. Madden and M. F. Hochella, Geochim. Cosmochim. Acta **69**, 389 (2005).
[15] L. E. Brus, J. Chem. Phys. **80**, 4403 (1984).
[16] S. U. M. Khan and J. Akikusa, J. Phys. Chem. B **103**, 7184 (1999).
[17] A. Fujimori, M. Saeki, N. Kimizuka, M. Taniguchi, and S. Suga, Phys. Rev. B **34**, 7318 (1986).
[18] D. M. Sherman, Phys. Chem. Miner. **12**, 161 (1985).
[19] J. Lüning, J. Rockenberger, S. Eisbitt, J. E. Rubensson, A. Karl, A. Kornowski, H. Weller, and W. Eberhardt, Solid State Commun. **112**, 5 (1999).
[20] C. L. Dong, P. Persson, L. Vayssieres, A. Augustsson, T. Schmitt, M. Mattesini, R. Ahuja, C. L. Chang, and J.-H. Guo, Phys. Rev. B **70**, 195325 (2004).
[21] D. M. Sherman, Geochim. Cosmochim. Acta **69**, 3249 (2005).
[22] F. M. F. de Groot, M. Grioni, J. C. Fuggle, J. Ghijsen, G. A. Sawatzky, and H. Petersen, Phys. Rev. B **40**, 5715 (1989).
[23] Z. Y. Wu, S. Gota, F. Jollet, M. Pollak, and M. Gautier-Soyer, Phys. Rev. B **55**, 2570 (1997).
[24] W. C. Mackrodt, F. Joliet, and M. Gautier-Soyer, Philos. Mag. B **79**, 25 (1999).
[25] E. Guiot, Z. Y. Wu, S. Gota, and M. Gautier-Soyer, J. Electron Spectrosc. Relat. Phenom. **101-103**, 371 (1999).
[26] L. X. Chen, T. Liu, M. C. Thurnauer, R. Csencsits, and T. Rajh, J. Phys. Chem. B **106**, 8539 (2002).
[27] J.-P. Jolivet, C. Chanéac, and E. Tronc, Chem. Commun. (Cambridge) **2004**, 481.
[28] T. Sugimoto, Y. Wang, H. Itoh, and A. Muramatsu, Colloids Surf., A **134**, 265 (1998).
[29] C. Frandsen, C. R. H. Bahl, B. Lebech, K. Lefmann, L. T. Kuhn, L. Keller, N. H. Andersen, M. von Zimmermann, E. Johnson, S. N. Klausen, and S. Morup, Phys. Rev. B **72**, 214406 (2005).

[30] A. P. Hammersley, *ESRF Internal Report*, ESRF98HA01T, FIT2D V9.129 Reference Manual V3.1, 1998).
[31] L. Lutterotti, D. Chateigner, S. Ferrari, and J. Ricote, Thin Solid Films **450**, 34 (2004).
[32] C. L. Farrow, P. Juhas, J. W. Liu, D. Bryndin, E. S. Bozin, J. Bloch, T. Proffen, and S. J. L. Billinge, J. Phys. Condens. Matter **19**, 335219 (2007).
[33] J. Nordgren and R. Nyholm, Nucl. Instrum. Methods Phys. Res. A **246**, 242 (1986).
[34] V. S. Lusvardi, M. A. Barteau, J. G. Chen, J. Eng, Jr., B. Frühberger, and A. Teplyakov, Surf. Sci. **397**, 237 (1998).
[35] B. Gilbert, J. Appl. Crystallogr. **41**, 554 (2008).
[36] X. Qiu, E. Bozin, P. Juhas, T. Proffen, and S. J. L. Billinge, J. Appl. Crystallogr. **37**, 110 (2004).
[37] D. M. Sherman and T. D. Waite, Am. Mineral. **70**, 1262 (1985).
[38] L. A. Marusak, R. Messier, and W. B. White, J. Phys. Chem. Solids **41**, 981 (1980).
[39] M. P. Dare-Edwards, J. B. Goodenough, A. Hamnett, and P. R. Trevell, J. Chem. Soc., Faraday Trans. I **79**, 2027 (1983).
[40] R. G. J. Strens and B. J. Wood, Mineral. Mag. **43**, 347 (1979).
[41] J. Wu, W. Walukiewisz, K. M. Yu, J. D. Denlinger, W. Shan, J. W. Ager, A. Kimura, H. F. Tang, and T. F. Kuech, Phys. Rev. B **70**, 115214 (2004).
[42] L. Weinhardt, O. Fuchs, E. Umbach, C. Heske, A. Fleszar, W. Hanke, and J. D. Denlinger, Phys. Rev. B **75**, 165207 (2007).
[43] A. Kotani and S. Shin, Rev. Mod. Phys. **73**, 203 (2001).
[44] L.-C. Duda, J. Nordgren, G. Drager, S. Bocharov, and T. Kirchner, J. Electron Spectrosc. Relat. Phenom. **110-111**, 275 (2000).
[45] S. M. Butorin, J.-H. Guo, M. Magnuson, P. Kuiper, and J. Nordgren, Phys. Rev. B **54**, 4405 (1996).
[46] Y. Ma, P. D. Johnson, N. Waasdahl, J. Guo, P. Skytt, J. Nordgren, S. D. Kevan, J. E. Rubensson, T. Böske, and W. Eberhardt, Phys. Rev. B **48**, 2109 (1993).
[47] K. C. Prince, F. Bondino, M. Zangrando, M. Zacchigna, K. Kuepper, M. Neumann, and F. Parmigiani, J. Electron Spectrosc. Relat. Phenom. **144-147**, 719 (2005).
[48] W. Y. Ching and Y.-N. Xu, J. Am. Ceram. Soc. **77**, 404 (1994).
[49] Y. Ma, N. Wassdahl, P. Skytt, J. Guo, J. Nordgren, P. D. Johnson, J.-E. Rubensson, T. Boske, W. Eberhardt, and S. D. Kevan, Phys. Rev. Lett. **69**, 2598 (1992).
[50] A. Agui, S. Shin, M. Fujisawa, Y. Tezuka, T. Ishii, Y. Muramatsu, O. Mishima, and K. Era, Phys. Rev. B **55**, 2073 (1997).
[51] V. N. Strocov, T. Schmitt, J.-E. Rubensson, P. Blaha, T. Paskova, and P. O. Nilsson, Phys. Status Solidi B **241**, R27 (2004).
[52] T.-Y. Chen, C.-H. Hsia, H. S. Son, and D. H. Son, J. Am. Chem. Soc. **129**, 10829 (2007).